Novel Dye-Sensitized Solar Cell Architecture Using TiO_2-Coated Vertically Aligned Carbon Nanofiber Arrays

Jianwei Liu,[†] Yen-Ting Kuo,[†] Kenneth J. Klabunde,[†] Caitlin Rochford,[‡] Judy Wu,[‡] and Jun Li*[,†]

Department of Chemistry, Kansas State University, Manhattan, Kansas 66506, and Department of Physics, University of Kansas, Lawrence, Kansas 66044

ABSTRACT A novel dye-sensitized solar cell (DSSC) architecture based on vertically aligned carbon nanofibers coated with a thin nanoneedle-textured anatase TiO_2 film is demonstrated. An encouraging overall conversion efficiency of ~1.09% and a rather high open-circuit voltage of ~0.64 V have been achieved. The efficient charge separation at the TiO_2–CNF junction and the large outer TiO_2 surface of this core–shell architecture provide new methods to tune the materials and interfaces in solar cells.

KEYWORDS: hybrid materials • solar cells • vertically aligned carbon nanofibers • coaxial core–shell nanowire

INTRODUCTION

New solar cell (SC) architectures that can be fabricated using nonconventional nanomaterials have attracted extensive attention in recent years because of the demand of photovoltaic technologies for large-scale energy production (1–3). Dye-sensitized SCs (DSSCs) that were originally constructed from a three-dimensional mesoporous network of TiO_2 nanoparticles (NPs) have appeared as a very promising low-cost technology (4). The ability to achieve an overall power conversion efficiency up to 10.4% (5) or even higher has stimulated extensive studies focused on understanding electron transport and how to reduce the charge recombination at the TiO_2 surface. One of the promising methods is to use vertically aligned TiO_2 nanotubes (NTs) (6, 7), ZnO nanowires (NWs) (8, 9), ZnO NTs (10), and Si NWs (11, 12) as direct electron pathways to facilitate faster transport. Here we report on a new architecture based on the coaxial coating of TiO_2 nanoneedles on a vertically aligned carbon nanofiber (VACNF) array. VACNFs are a subset of multiwalled carbon NTs (MWCNTs) grown by plasma-enhanced chemical vapor deposition (PECVD) on solid substrates (13). The electric field during PECVD growth assists the vertical alignment and results in a uniform nanobrushlike structure free-standing on solid substrates (14–17). We demonstrate that the unique VACNF structure can be used as a highly conductive nanostructured core to collect electrons in a DSSC on which a nanoneedle-textured anatase TiO_2 shell is coated as the charge separation barrier. This architecture provides the capability of studying the effect of the electron collection and charge separation in the DSSC processes by separately tuning the core–shell materials.

Recently, we demonstrated that a particulated anatase TiO_2 film can be deposited on a VACNF array by a metal–organic chemical vapor deposition (MOCVD) strategy to form a coaxial core–shell NW array structure (13). Interestingly, the TiO_2 particles in the film elongate into densely stacked nanoneedles when the deposition time is increased over 30 min. This provides a large TiO_2 outer surface, which is desired for increasing dye adsorption. Photoluminescence analysis indicates the complete fluorescence quenching of TiO_2 excitation due to electron separation at the TiO_2 to carbon nanofiber (CNF) heterojunction, which is homogeneously formed around each CNF (13). Here, we demonstrate the successful fabrication of a DSSC using such a nanostructured core–shell architecture. An encouraging overall power conversion efficiency of 1.09% and a relatively high open-circuit voltage (V_{oc}) of 0.64 V have been achieved. This provides a new architecture beyond TiO_2/ZnO core–shell NW arrays (18), which allows further study of the effect of the materials and interface properties on electron transfer in such structures.

EXPERIMENTAL SECTION

Preparation of DSSC Photoanodes. The preparation of DSSC photoanodes in this study consists of three steps. First, the fluorine-doped tin oxide (FTO) was deposited on 1.0-mm-thick quartz slides with a size of 2 cm × 2 cm by spray pyrolysis of a mixture solution in air (19). The solution consisted of $SnCl_4 \cdot 5H_2O$ (2.80 g) dissolved in ethanol (40 mL), which was then mixed with a saturated aqueous solution of NH_4F (0.48 g), followed by sonication for ~20 min. It was atomized by compressed air at a pressure of 0.06 MPa through an airbrush onto the substrate at 410 °C. After 45 min of deposition, a FTO film of 15 μm thickness was obtained with a sheet resistance comparable to that of commercial FTO anodes from Solaronix. Second, VACNF arrays were grown on the substrates at ~800 °C with a direct-current-biased PECVD system (AIXTRON) following previously published procedures (14–17) using a 22-nm-thick Ni catalyst film and a mixture of C_2H_2 and NH_3 as the

* To whom correspondence should be addressed. E-mail: junli@ksu.edu. Tel: (785) 532-0955.
Received for review May 11, 2009 and accepted July 14, 2009
[†] Kansas State University.
[‡] University of Kansas.
DOI: 10.1021/am900316f

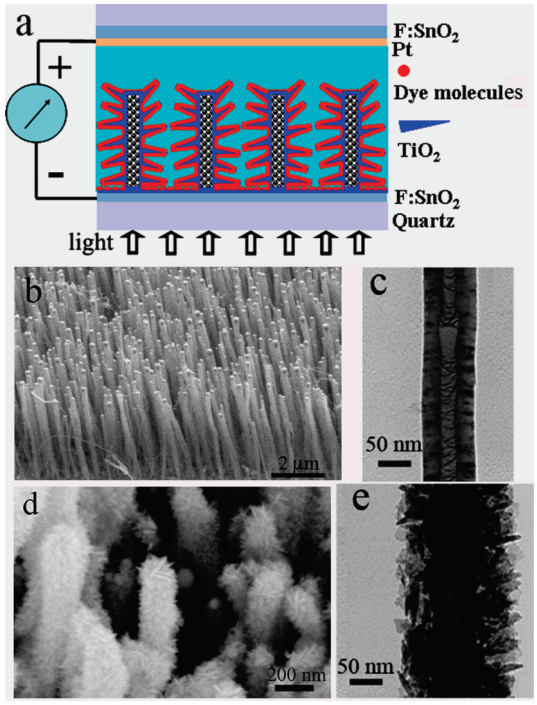

FIGURE 1. (a) Schematic of VACNF arrays coated with anatase TiO_2 nanoneedles for DSSCs. (b) SEM image at a 45° perspective view of an as-grown VACNF array. (c) TEM image of an as-grown CNF. (d) SEM image at a 45° perspective view of the VACNF array after being coated with anatase TiO_2 nanoneedles. (e) TEM image of a CNF after being coated with anatase TiO_2 nanoneedles.

gas precursors. Third, a TiO_2 layer was deposited on the VACNF array via MOCVD using titanium isopropoxide vapor under 150 mTorr at 550 °C.

Fabrication and Characterization of DSSCs. The DSSCs were prepared by immersion of the bare or TiO_2-coated VACNF array in a 0.2 mM ethanol solution of *cis*-bis(isothiocyanoto)bis(2,2′-bipyridyl-4,4′-dicarboxylato)ruthenium(II) bis(tetrabutylammonium) dye (N719, Solaronix) for 12 h. Sensitized anodes were then bonded with thermally platinized FTO/glass cathodes with a hot melt spacer (60 μm thick, Solaronix). The electrolyte (Iodolyte AN-50, Solaronix) consisting of 50 mM triiodide, 0.1 M LiI, and 0.5 M 1,2-dimethyl-3-propylimidazolium iodide in acetonitrile was filled in the cell by capillary forces. The cells with an active area of 1 cm × 1 cm were tested under one sun AM 1.5G simulated sunlight (300 W ozone-free Xe lamp, Newport 67005 Lamp Housing). The current−voltage (I−V) data were recorded with a potentiostat (model 440A, CH Instruments) and validated with a standard Si SC to avoid the possible error due to the additional power extracted from the potentiostat.

RESULTS AND DISCUSSION

VACNFs present an extraordinary vertical alignment distinct from other CNT materials. As shown in Figure 1b, each CNF free-stands on the substrate surface with the Ni catalyst particle present at the tip. The diameter of CNFs can be controlled from 50 to 100 nm, and the length can be varied from a few micrometers to ~40 μm. The well-defined vertical alignment and lower growth temperature provided by PECVD make VACNF arrays more attractive than randomly stacked CNTs for SC applications. The intrinsic resistivity of CNFs was previously found to be $\rho = 0.4-7$ mΩ cm (20−22), a few hundred times lower than that of ZnO NW (~0.3−2.0 Ω cm) (9), making them a better electron collector in NW-based DSSCs. The work function of CNFs is presumably similar to that of graphite (at ~4.5−5.0 eV), matching well with that of the commonly used transparent conductive electrodes (TCEs) such as indium-doped tin oxide (ITO) or FTO. The bamboolike structure shown in Figure 1c is the characteristic signature of this material, differentiating it from MWCNTs. Under proper conditions (MOCVD for 60 min) (13), the TiO_2 film forms an interesting nanoneedle-like texture uniformly wrapping around each CNF, as shown by both scanning electron microscopy (SEM) and transmission electron microscopy (TEM) images in Figure 1d,e, which provides the desired large TiO_2 surface for dye adsorption in DSSC fabrication.

So far, all VACNF arrays have been fabricated on opaque substrates (mostly on Si) using PECVD (14−17). The SC architecture shown in Figure 1a requires the growth of VACNF arrays on TCEs. We prepared FTO electrodes on quartz as substrates in this study. In the future, it is possible to lower the PECVD growth temperature below ~500 °C, i.e., the melting point of glass (the common photoanode substrates) (14, 17).

Figure 1b shows a SEM image at a 45° perspective view of an as-grown VACNF array of ~5 μm in length with a rather uniform vertical alignment. The density is ~$1-2 \times 10^9$ CNF/cm^2, corresponding to an average nearest-neighbor distance of ~300−400 nm. Such three-dimensional nanobrush structures offer sufficient open space for TiO_2 and dye molecule deposition. As we reported before (13), TiO_2 forms a conformal particulated film of anatase crystal structure around individual CNFs by the MOCVD process within ~30 min of deposition. With a longer deposition time of ~60 min, the TiO_2 particles elongated into nanoneedles stacked on the CNF surface, with an average diameter of 10−15 nm and a length of 50−100 nm (Figure 1d,e). This gives a much larger surface area than the smooth ZnO NWs and TiO_2 NTs (5−8). More dye molecules can be adsorbed, which is desired for higher DSSC efficiency. All TiO_2 coatings in this study are based on such a nanoneedle-textured structure fabricated with a 60-min MOCVD process.

The strong light absorption by carbon materials (23, 24) such as CNTs and CNFs in the UV−vis range has been a concern in their applications as photoanodes in SCs. This appeared not to be a significant factor for the VACNF architecture, as demonstrated with transmission UV−vis−IR optical spectroscopic measurements. Figure 2a shows the transmittance spectra (Cary 500 UV−vis−near-IR spectrophotometer, wavelength from 200 to 2200 nm) of the homemade FTO/quartz substrate in comparison with the commercial FTO/glass and ITO/glass electrodes as references (Solaronix). The transmittance is similar in the visible range among all samples, with a value between 63% and 78%. Higher transmittance is obtained with the homemade FTO/quartz sample at both UV and IR regions, giving some advantages for more light to pass through.

Figure 2b shows the transmittance spectra of the VACNF arrays with lengths of 1, 2.5, and 5 μm, respectively. The 1-μm-long VACNF array shows rather high transmittance

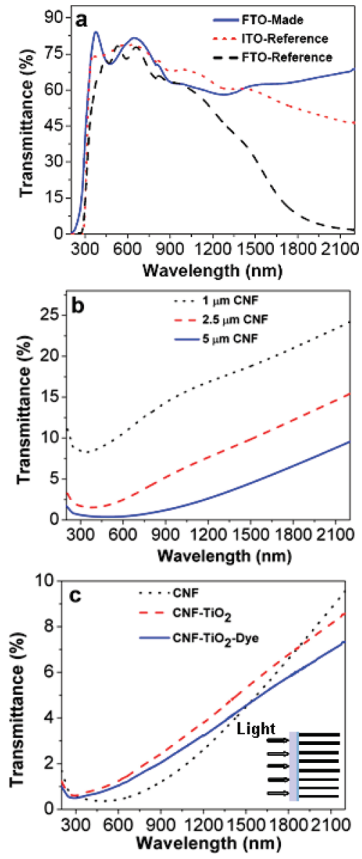

FIGURE 2. (a) Transmission optical spectra of a homemade FTO film on quartz substrates in comparison with references, i.e., commercial FTO and ITO films on glass substrates. (b) Transmission optical spectra of VACNF arrays with lengths of 1, 2.5, and 5 μm, respectively. (c) Transmission optical spectra of 5-μm-long as-grown VACNF arrays, after being coated with TiO_2 and further derivatization with N-917 ruthenium dye molecules. The inset in part c shows the configuration for measurements with the light shining perpendicular to the substrate surface.

over the whole spectrum with a minimum transmittance of ~8.18% at a wavelength of ~320 nm. The transmittance increases as the wavelength moves to the visible and IR regions. As the length of the VACNF increases, the minimum transmittance is lowered to 1.51% and shifts to longer wavelength at ~400 nm for 2.5 μm VACNF arrays. It is further lowered to 0.36% at ~500 nm for 5.0 μm VACNF arrays. Even though the transmittance decreases as the length of the CNF is increased, more than 0.36% of light can penetrate through the 5.0-μm-long VACNF array in the visible range. This indicates an optical penetration depth of ~5 μm, only slightly smaller than the 10-μm penetration depth in conventional TiO_2 NP-based DSSCs (25).

The small light absorption by VACNF arrays is in drastic contrast to other studies using random CNT networks laterally stacked on the substrate surface (26, 27) or high-density entangled CNT vertical structures (28). This allows the use of CNFs as thick as 5 μm instead of a few hundred nanometers. A perfect VACNF array with ~100 nm diameter and a density of 1×10^9 CNF/cm^2 should have a footprint only accounting for about 8% of the surface area. Therefore, 92% of the light should pass through a VACNF array of any length if it shines perpendicularly to the surface. However, the produced VACNFs have small random tilt at an angle within ±10° from the surface normal, which generates a much larger projected area on the substrate surface, in proportion to the CNF length. Assuming that all CNFs are tilted in the same direction by 10° from the surface normal, the projected footprint of 5-μm-long VACNFs will cover nearly 100% of the surface, which is close to our experimental results.

Interestingly, we found that the phototransmittance by VACNFs can be significantly increased after coating with TiO_2 and organometallic dyes, respectively. Figure 2c shows the transmittance spectra of the 5-μm-long VACNF array at three different conditions. The wavelength of minimum transmittance shifted from ~500 to ~300 nm, and the minimum transmittance value is increased from ~0.36% to 0.60% after coating with TiO_2. This may be attributed to the strong scattering by the rough TiO_2 surface. The transmittance in the visible range is increased even more. After application of the dye molecules, the transmittance slightly decreases over the entire spectrum with a minimum value of ~0.50%, attributing to the additional absorption by the monolayer of dye molecules on the TiO_2 surface. In optimization of the DSSC efficiency, the TiO_2 surface should be derivatized with dyes (29) or quantum dots (30) with higher absorption coefficients so that the loss of photons due to CNF absorption can be reduced.

The $I-V$ characteristics of DSSCs constructed with an as-grown VACNF array and a TiO_2-coated VACNF as anodes are shown in Figure 3a. The DSSC made of a TiO_2-coated VACNF array shows a short-circuit current (J_{sc}) of 2.91 mA/cm^2 and an open-circuit voltage (V_{oc}) of 0.640 V. A fill factor (FF) of 58.2% is obtained at the circuit voltage of 0.462 V, which corresponds to a maximum overall efficiency (η) of 1.09%. These performance parameters are close to those of the DSSCs using vertical TiO_2 NTs (7), ZnO NWs/NTs (8, 9), ZnO−TiO_2 core−shell NW structures (18), and non-$TiCl_4$-treated TiO_2 NPs (6) but better than those of the DSSCs fabricated with TiO_2 NPs deposited on single-walled CNT (SWCNT) scaffolds (27). To our surprise, even the DSSC fabricated with an as-grown VACNF array presents photovoltaic effects with $J_{sc} = 0.216$ mA/cm^2, $V_{oc} = 0.550$ V, FF = 20.7%, and maximum efficiency $\eta = 0.025$%, respectively. Clearly, electrons can be directly transferred from ruthenium dyes to CNFs, indicating the good electron collection capability of the VACNF template. The significantly enhanced efficiency after coating of the bare VACNFs with the TiO_2 film indicates that the TiO_2 layer is necessary as an energy barrier for improving the separation of photoexcited electrons from oxidized dye molecules (18). Electrons are then collected by the highly conductive CNF cores, while the dyes carrying the produced holes remain at the external TiO_2 surface and are quickly reduced to the original state by reaction with iodide ions in the solution. The rough surface of the TiO_2 nanoneedle texture is expected to provide a larger effective surface area to support the dye absorption, approaching that of the traditional TiO_2 NP-based DSSCs (4, 5).

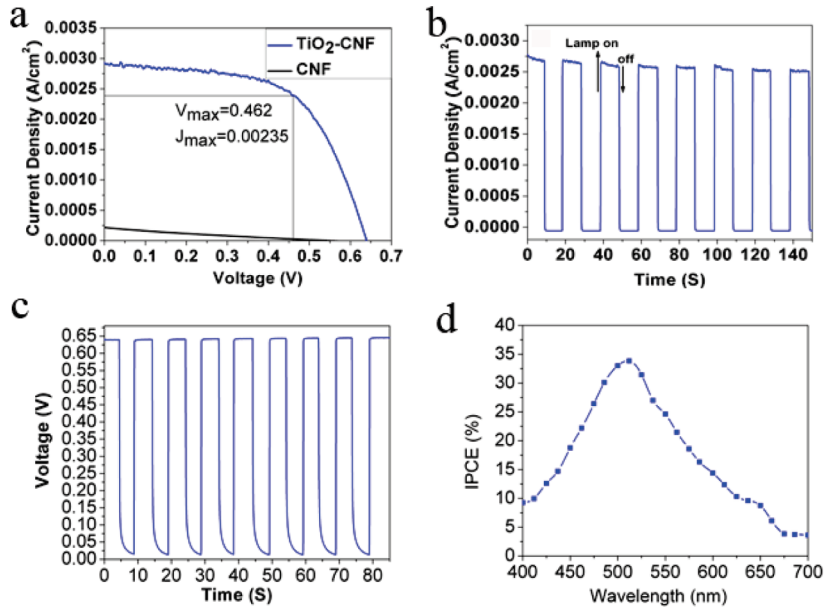

FIGURE 3. (a) Current−voltage characteristics of DSSCs constructed with as-grown VACNFs (black line) and TiO_2-coated VACNFs (blue line). The current density (J_{max} in A/cm^2) and voltage (V_{max} in V) of the TiO_2-coated VACNF SC at maximum conversion efficiency are shown in the figure. (b) Photocurrent response (i.e., short-circuit current J_{sc}) of the DSSC constructed using TiO_2-coated VACNFs during light ON−OFF cycles. (c) Photovoltage response (i.e., open-circuit voltage V_{oc}) during light ON−OFF cycles. (d) Photocurrent action spectra of DSSC. IPCE (%) = $1240J_{sc}/\lambda \mathbf{I}_{inc} \times 100$, where J_{sc} is the short-circuit current and I_{inc} is the power of the incident light.

Law et al. (18) have previously demonstrated that applying a TiO_2 shell of 10−25 nm thickness on a ZnO NW array core caused a dramatic increase in V_{OC} and FF. This was attributed to the suppression of the interfacial recombination of the TiO_2 shells. An energy barrier of ϕ_{bi} = 75−150 mV was expected based on the likely doping difference between the ZnO core and the TiO_2 shell. This radial field would reduce the electron concentration at the outer surface of the NW by a factor of $\exp(-\phi_{bi}/kT)$, or roughly 20−300 times smaller than the center of the NW. This concept can be also applied in this study using the TiO_2 shell on the CNF core. In previous studies (20, 21), we have demonstrated that all CNFs present metallic properties similar to those of graphite. The work function of CNF is expected to be similar to that of graphite with a value of 4.5 to 5.0 eV. The difference between the Fermi level of CNFs and the conduction band edge of TiO_2 shell is expected to result in a potential difference of −200 to −700 mV at the CNF−TiO_2 interface, which is much larger than that at the ZnO−TiO_2 interface. We expect that this large potential difference will be more effective in suppressing the charge recombination at the outer TiO_2 surface, as demonstrated by the much higher energy conversion efficiency with the TiO_2−CNF DSSC than the CNF DSSC. The main potential advantage of TiO_2−VACNF architecture is that it combines three desired properties for a highly efficient DSSC, i.e., an efficient charge separation with the TiO_2 shell as an energy barrier, a large effective surface area by a nanoneedle-like TiO_2 texture, and a fast electron transport through the highly conductive metallic CNF core. This report demonstrates that a working DSSC with reasonable efficiency can be fabricated with the VACNF−TiO_2 core−shell architecture. The optimization of the efficiency and the study of the charge-transfer rate at each interface (particularly with time-resolved measurements) must to be carried out in the future to realize all of these potentials.

In addition, we found that the short-circuit photocurrent J_{sc} showed reproducible responses during ON−OFF cycles. As illustrated in Figure 3b, the initial J_{sc} of a DSSC with TiO_2−VACNF architecture is ∼2.75 mA/cm^2. It monotonically decreases versus time when the light is turned on. The photocurrent instantaneously drops to zero when the light is turned off and is able to recover the previous level after the light is turned back on. After about 30 s of light exposure, J_{sc} becomes stabilized at a value of ∼2.50 mA/cm^2, which is about 93% of the initial value. It then remains at this level for about 3 min, while the light is cycled between ON and OFF every 10 s until the experiment is stopped. Stability tests with longer time scales will be pursued in the future. In the meantime, the open-circuit voltage V_{oc} showed very reproducible responses during ON−OFF cycles, as seen in Figure 3c.

Furthermore, we evaluated the DSSC performance by recording the incident photon-to-charge carrier conversion efficiency (IPCE) at different incident wavelengths, as shown in Figure 3d. The IPCE was calculated by IPCE (%) = $1240J_{sc}/\lambda I_{inc} \times 100$, where I_{inc} is the power of the incident light (26). Clearly, an IPCE maximum at 515 nm correlates well with the peak absorption of the ruthenium(II) dye. A maximum photoconversion efficiency of 34% was achieved, which is comparable with that of DSSCs made of ZnO_2 NT arrays (∼35%) (10) but higher than that of TiO_2 NPs on SWCNTs (∼15% (26) to 25% (27)). This value, however, is likely limited by the ruthenium(II) adsorption on the surface of a TiO_2-coated VACNF array, which needs to be optimized in the future. Quantitative characterization of the uptake of ruthenium(II) is in process.

Our results not only indicate that the fabrication of VACNF-supported TiO_2−CNF core−shell DSSCs is feasible but also demonstrate an encouraging $I-V$ characteristic. For comparison, we also fabricated a DSSC with a 10-μm-thick film of TiO_2 NPs (15 nm diameter) using conventional methods with the same dye (N719) and the same electrolyte. We obtained similar $I-V$ characteristics with slightly higher energy conversion efficiency ($\eta = 1.86\%$) than the VACNF−TiO_2 core−shell DSSC ($\eta = 1.09\%$). This value is lower than the state-of-the-art efficiency of 10.4% reported in the literature (5) but is comparable to that in another study using TiO_2 NPs without $TiCl_4$ treatment (17). This side-by-side comparison implies that the efficiency of our DSSCs is not limited by the intrinsic material properties of the vertical architecture. Optimization of the preparation conditions by exploring various surface treatments is in progress to achieve the intrinsic efficiency that this architecture may offer.

Even though not yet optimized, the performance of the TiO_2−VACNF DSSCs has already surpassed that of other DSSCs fabricated with CNTs. Our study is consistent with the study by Kamat et al. using TiO_2 NPs on a dense randomly stacked SWCNT network (26, 27) in showing that CNTs or CNFs facilitate charge transport and improve DSSC photocurrent generation. However, the open-circuit voltage ($V_{oc} = \sim 0.26$ V) by Kamat et al. strangely decreased by more than 30% compared to the traditional DSSCs made with TiO_2 NPs alone (27). This was attributed to a significant positive shift in the apparent Fermi level of SWCNT photoanodes. The high V_{oc} (~0.65 V) in our study reported here reveals that this is not due to the intrinsic properties of CNTs or CNFs. Instead, the heterogeneous interfaces between the SWCNT scaffold and the bulk TiO_2 NP layer may be the real reason for the low V_{oc} in the previous study (27). The intact coating of a uniform TiO_2 layer coaxially around each CNF may facilitate a homogeneous TiO_2−CNF interface and thus enhance the performance.

CONCLUSIONS

In conclusion, we have demonstrated the successful fabrication of DSSCs based on the architecture of VACNF nanobrushs coated with a nanoneedle-textured anatase TiO_2 film. The VACNF array was grown on a transparent electrode consisting of a FTO film on quartz. Optical spectra indicate that VACNF has much less light absorption because of the vertically aligned structure. This ensures that the light can reach a much larger volume of active photovoltaic materials. TiO_2 coating and dye derivatization further enhance the utilization of photons at the TiO_2 shell surface and reduce the loss of photons by CNF absorption. The enhanced optical depth allows the use of a 5-μm-long VACNF array for DSSCs. The $I-V$ characterization under 100 mW/cm^2 sunlight gives an encouraging overall conversion efficiency of 1.09% and a rather high V_{oc} of 0.64 V comparable to those of DSSCs made with ZnO or TiO_2 NWs/NTs. This new core−shell vertical architecture presents a large open spacing, allowing homogeneous dye derivatization, quantum dots attachment, and mediator/electrolyte access. The ability to separate multiple roles in a DSSC by integrating various materials on the VACNF template provides new routes to investigating the mechanisms in solar energy capture and conversion. Optimization is in process to reach the intrinsic performance that this architecture may offer.

Acknowledgment. J.L. thanks Kansas State University for financial support.

REFERENCES AND NOTES

(1) Lewis, N. S. *Science* **2007**, *315*, 798.
(2) Huynh, W. U.; Dittmer, J. J.; Alivisatos, A. P. *Hybrid Nanorod−polym. Solar Cells Sci.* **2002**, *295*, 2425.
(3) *Basic Energy Needs for Solar Energy Utilization; Basic Energy Science*; U.S. Department of Energy: Washington, DC, Apr 2005, pp 57−73.
(4) Oregan, B.; Gratzel, M. *Nature* **1991**, *353*, 737.
(5) Hagfeldt, A.; Gratzel, M. *Acc. Chem. Res.* **2000**, *33*, 269.
(6) Mor, G. K.; Shankar, K.; Paulose, M.; Varghese, O. K.; Grimes, C. A. *Nano Lett.* **2006**, *6*, 215.
(7) Zhu, K.; Neale, N. R.; Miedaner, A.; Frank, A. J. *Nano Lett.* **2007**, *7*, 69.
(8) Baxter, J. B.; Aydil, E. S. *Appl. Phys. Lett.* **2005**, *86*, 053114.
(9) Law, M.; Greene, L. E.; Johnson, J. C.; Saykally, R.; Yang, P. D. *Nat. Mater.* **2005**, *4*, 455.
(10) Martinson, A. B. F.; Elam, J. W.; Hupp, J. T.; Pellin, M. J. *Nano Lett.* **2007**, 2183.
(11) Maiolo, J. R.; Kayes, B. M.; Filler, M. A.; Putnam, M. C.; Kelzenberg, M. D.; Atwater, H. A.; Lewis, N. S. *J. Am. Chem. Soc.* **2007**, *129*, 12346.
(12) Goodey, A. P.; Eichfeld, S. M.; Lew, K. K.; Redwing, J. M.; Mallouk, T. E. *J. Am. Chem. Soc.* **2007**, *129*, 12344.
(13) Liu, J. W.; Li, J.; Sedhain, A.; Lin, J. Y.; Jiang, H. X. *J. Phys. Chem. C* **2008**, *112*, 17127.
(14) Ren, Z. F.; Huang, Z. P.; Xu, J. W.; Wang, J. H.; Bush, P.; Siegal, M. P.; Provencio, P. N. *Science* **1998**, *282*, 1105.
(15) Cruden, B. A.; Cassell, A. M.; Ye, Q.; Meyyappan, M. *J. Appl. Phys.* **2003**, *94*, 4070.
(16) Melechko, A. V.; Merkulov, V. I.; McKnight, T. E.; Guillorn, M. A.; Klein, K. L.; Lowndes, D. H.; Simpson, M. L. *J. Appl. Phys.* **2005**, *97*, 41301.
(17) Haque, M. S.; Teo, K. B. K.; Rupensinghe, N. L.; Ali, S. Z.; Haneef, I.; Maeng, S.; Park, J.; Udrea, F.; Milne, A. I. *Nanotechnology* **2008**, *19*, 5.
(18) Law, M.; Greene, L. E.; Radenovic, A.; Kuykendall, T.; Liphardt, J.; Yang, P. D. *J. Phys. Chem. B* **2006**, *110*, 22652.
(19) Kawashima, T.; Ezure, T.; Okada, K.; Matsui, H.; Goto, K.; Tanabe, N. *J. Photochem. Photobiol. A: Chem.* **2004**, *164*, 199.
(20) Li, J.; Ye, Q.; Cassell, A.; Ng, H. T.; Stevens, R.; Han, J.; Meyyappan, M. *Appl. Phys. Lett.* **2003**, *82*, 2491.
(21) Ngo, Q.; Cassell, A. M.; Austin, A. J.; Li, J.; Krishnan, S.; Meyyappan, M.; Yang, C. Y. *IEEE Electron Device Lett.* **2006**, *27*, 221.
(22) Zhang, L.; Austin, D.; Merkulov, V. I.; Meleshko, A. V.; Klein, K. L.; Guillorn, M. A.; Lowndes, D. H.; Simpson, M. L. *Appl. Phys. Lett.* **2004**, *84*, 3972.
(23) de Heer, W. A.; Bacsa, W. S.; Chatelain, A.; Gerfin, T.; Humphrey-baker, R.; Forro, L.; Ugarte, D. *Science* **1995**, *268*, 845.
(24) Theocharous, E.; Deshpande, R.; Dillon, A. C.; Lehman, J. *Appl. Opt.* **2006**, *45*, 1093.
(25) Lee, J. J.; Goia, G. M.; Lewis, N. S. *J. Phys. Chem. B* **2004**, *108*, 5282.
(26) Kongkanand, A.; Dominguez, R. M.; Kamat, P. V. *Nano Lett.* **2007**, *7*, 676.
(27) Brown, P.; Takechi, K.; Kamat, P. V. *J. Phys. Chem. C* **2008**, *112*, 4776.
(28) Miller, A. J.; Hatton, R. A.; Chen, G. Y.; Silva, S. R. P. *Appl. Phys. Lett.* **2007**, *90*, 023105.
(29) Shankar, K.; Bandara, J.; Paulose, M.; Wietasch, H.; Varghese, O. K.; Mor, G. K.; LaTempa, T. J.; Thelakkat, M.; Grimes, C. A. *Nano Lett.* **2008**, *8*, 1654.
(30) Kongkanand, A.; Tvrdy, K.; Takechi, K.; Kuno, M.; Kamat, P. V. *J. Am. Chem. Soc.* **2008**, *130*, 4007.

AM900316F